Supporting Information

Covalent organic framework-derived CoRu nanoalloy doped macro-microporous carbon for efficient electrocatalysis

Huihui Zhao,[a] Xinghao Zhang,[a] Yaowen Zhang,[b] Yuzhuang Song,[a] Chen Li,[a] Kang Liu,*[a] and Dingxuan Ma*[a]

[a] College of Chemistry and Molecular Engineering, Key Laboratory of Optic-Electric Sensing and Analytical Chemistry for Life Science, Qingdao University of Science and Technology, Qingdao 266042, P. R. China.

[b] State Key Laboratory of Inorganic Synthesis and Preparative Chemistry, College of Chemistry, Jilin University, Changchun 130012, P. R. China.

E-mail: madingxuan640@126.com, liukang82@126.com

Contents:

1. Materials and Instrumentation

All reagents used in the syntheses were commercially available and used without further purification. Powder X-ray diffraction (PXRD) was performed with a Rigaku D/MAX2550 diffractometer. Scanning electron microscopy (SEM) was performed on JSM-7500F. Transmission electron microscopy (TEM) was performed on FEI Tecnai G2 S-Twin with a field emission gun operating at 200 kV. Images were acquired digitally on a Gantan multiple CCD camera. Energy dispersive spectroscopy (EDS) spectra were obtained using a JEOL JSM-6300 at 5 kV. Gas adsorption experiments were carried out on a Micrometrics ASAP 2020M volumetric gas adsorption analyzer. Inductively coupled plasma-optical emission spectrometry (ICP-OES) was carried out on an Agilent 730. Raman spectra were measured by inVia Reflex. X-ray photoelectron spectroscopy (XPS) measurements were performed on an ESCALAB 250 X-ray photoelectron spectroscopy, using Mg Kα X-ray as the excitation source. The X-ray absorption data at the Co *K*-edge of the samples were recorded at beam line BL14W1 of the Shanghai Synchrotron Radiation Facility (SSRF), China.[1]

2. Synthetic Procedures

2.1 Synthesis of PS template

Monodisperse colloidal PS spheres (~200 nm) can be achieved according to the related literature.[2] In a typical procedure, 39 mL of styrene was washed with 12 mL NaOH aqueous solution (10 wt%) and subsequently deionized water to remove the stabilizer. Then styrene and 1.5 g polyvinyl pyrrolidone (PVP, Mw~29000) were added to a round-bottom flask containing 300 mL water. The mixture was bubbled with N_2 for 15 min and the mixture was heated at 90 °C for 30 min under magnetic stirring. Then, 50 mL water with 0.5 g $K_2S_2O_8$ was added into the flask to initiate the polymerization of styrene. After keep stirring (<500 r.p.m.) for 24 h at this temperature, monodisperse colloidal PS spheres were formed.

2.2 Synthesis of PS@COF-SO_3NH_4

p-Toluenesulfonic acid (1.45 mmol, 250 mg), 2,5-diaminobenzenesulfonic acid (0.225 mmol, 42.3 mg) and 2.5 mL colloidal PS were mixed thoroughly into a 20 mL disposable scintillation vial shaker for 30 min. 1,3,5-Triformylphloroglucinol (0.15 mmol, 31.5 mg) was added and the vial was further shaken for 30 minutes. The solution was transferred to an open petri dish to evaporate the water, and then transferred into an oven at 80 ℃ for 24 h. The afforded solid content, was thoroughly washed with hot water to remove *p*-toluenesulfonic acid and subsequently washed with ethanol, and dried in vacuum at 60 °C to afford PS@COF-SO_3H. PS@COF-SO_3NH_4 was synthesized by soaking 200 mg PS@COF-SO_3H in ammonia water (1 wt%) 40 mL and further stirring for 30 h. Then the solid was filtered and washed with a large amount of deionized water and methanol. The PS@COF-SO_3NH_4 was finally obtained after drying overnight in a vacuum oven at 60 °C.

2.3 Synthesis of m-CoRu@NC

65 mg PS@COF-SO_3NH_4, 10 mg $Co(CH_3COO)_2{\cdot}4H_2O$ and 10 mg $RuCl_3{\cdot}3H_2O$ were ultrasonically dissolved in 15 mL deionized water, and further stirring for 12 h to conduct ion exchange. After that, the obtained solid was filtered and washed with deionized water and methanol, and PS@COF-SO_3CoRu was obtained after dried overnight at 60 ℃ under vacuum. The thermal decomposition of COF precursor was performed at 300 ℃ under N_2 atmosphere for 1 h with a heating rate of 10 ℃ min^{-1}, and further heated up to 550 ℃ with the same rate for 4 h.

2.4 Synthesis of m-Co@NC and m-Ru@NC

The synthetic process is similar with the m-CoRu@NC, except for only using $Co(CH_3COO)_2{\cdot}4H_2O$ or $RuCl_3{\cdot}3H_2O$ during the ion exchange.

3. Characterization

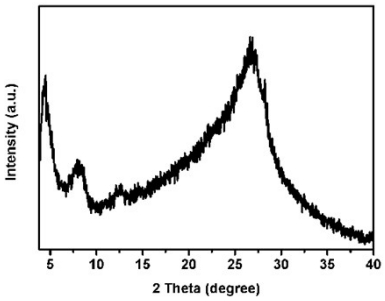

Figure S1. Power XRD pattern of PS@COF-SO_3NH_4.

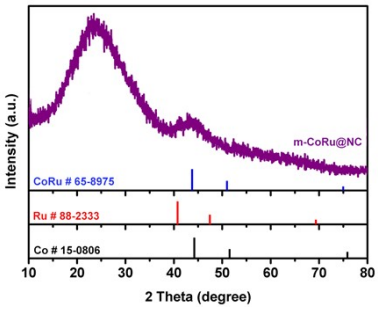

Figure S2. Power XRD pattern of m-CoRu@NC.

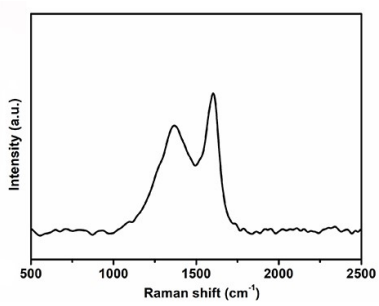

Figure S3. Raman spectra of m-CoRu@NC.

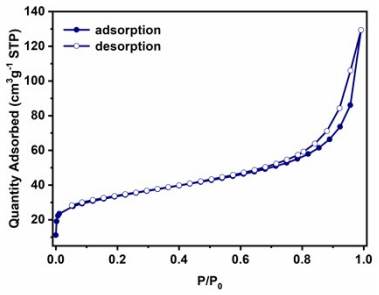

Figure S4. N_2 adsorption and desorption isotherms of m-CoRu@NC.

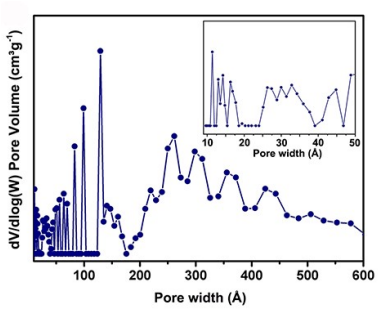

Figure S5. Pore-size distribution profiles of m-CoRu@NC.

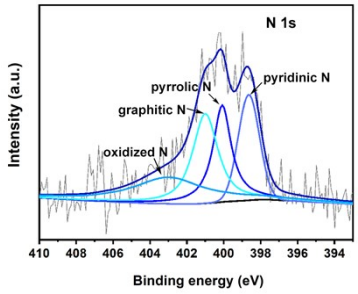

Figure S6. N 1s XPS spectra of m-CoRu@NC.

4. Electrochemical measurements

All electrochemical tests were measured on an electrochemical work station (CHI760E Shanghai, Chenhua) with representative three-electrode configuration. A polished glassy carbon electrode (GC) was used as the working electrode (3 mm diameter, 0.07065 cm^2), a platnum electrode was served as the counter electrode and the saturated calomel electrode (SCE) acted as the reference electrode. The catalyst ink was prepared as follows: 5 mg of catalyst powder, 400 μL water, 560 μL ethanol and 40 μL 5 wt% Nafion were mixed ultrasonically for 30 min. Then, 5 μL catalyst ink was dropped on the glassy carbon electrode to form a catalyst film with a catalyst loading of 0.34 mg cm^{-2}. The catalytic activity was measured in 1.0 M KOH solution. Linear sweep voltammetry was performed at the range of -1 V to -1.7 V and 0 V to 0.8 V at 5 mV s^{-1} without iR compensation. In the work, according to calibration E_q to reversible hydrogen electrode conversion for all potentials ($E_{RHE} = E_{SCE} + 0.059 \times pH$). The electrochemical active surface area (ECSA) of electrocatalyst was determined by double-layer capacitance (C_{dl}), whose values can be obtained from cyclic voltammetry under different scan rates of 20, 40, 60, 80, 100 and 120 mV s^{-1}. EIS was test on Gamry Reference 600+. Overall water splitting was measured in a two-electrode configuration by uniformly dropped 140 μL catalyst ink on a nickel foam electrode (1×2 cm^2).

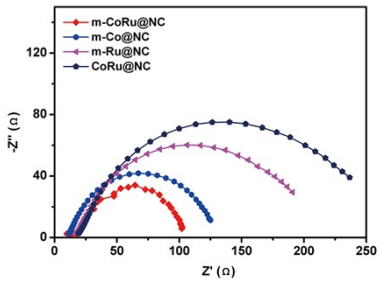

Figure S7. The EIS of m-CoRu@NC, m-Co@NC, m-Ru@NC and CoRu@NC.

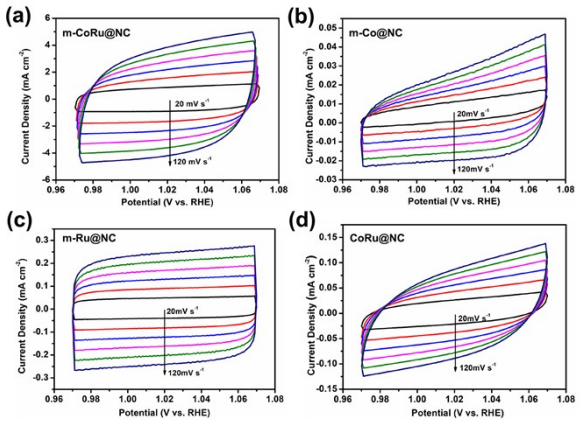

Figure S8. CV curves of (a) m-CoRu@NC, (b) m-Co@NC, (c) m-Ru@NC and (d) CoRu@NC with different scan rates from 20 to 120 mV s^{-1}, during HER process under 1.0 M KOH solution.

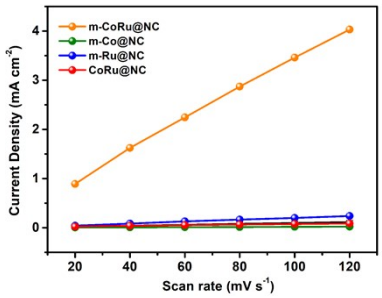

Figure S9. The double-layer capacitance (C_{dl}) values of m-CoRu@NC, m-Co@NC, m-Ru@NC and CoRu@NC during HER process under 1.0 M KOH solution.

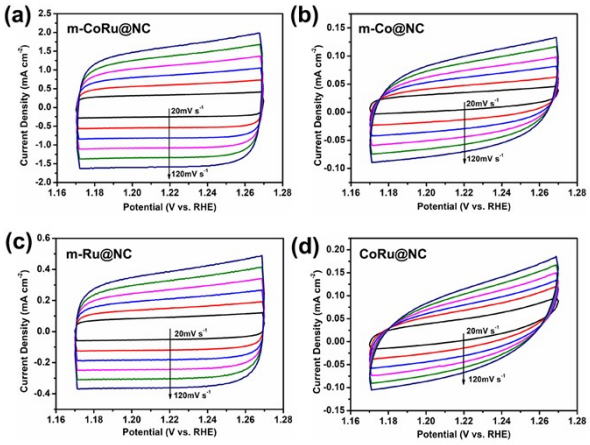

Figure S10. CV curves of (a) m-CoRu@NC, (b) m-Co@NC, (c) m-Ru@NC and (d) CoRu@NC with different scan rates from 20 to 120 mV s^{-1}, during OER process under 1.0 M KOH solution.

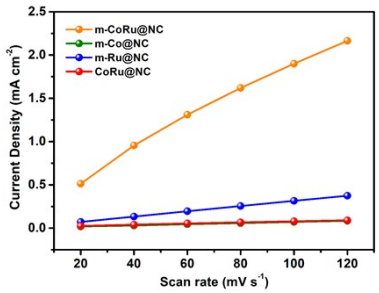

Figure S11. The double-layer capacitance (C_{dl}) values of m-CoRu@NC, m-Co@NC, m-Ru@NC and CoRu@NC during OER process under 1.0 M KOH solution.

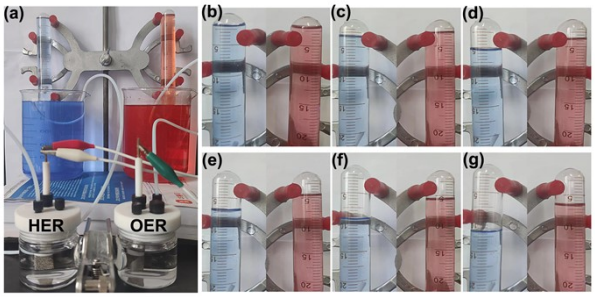

Figure S12. (a) The photo for measuring Faraday efficiency of device. Gas collected at different times (b) 0 s, (c) 180 s, (d) 540 s, (e) 900 s, (f) 1260 s, (g) 1620 s.

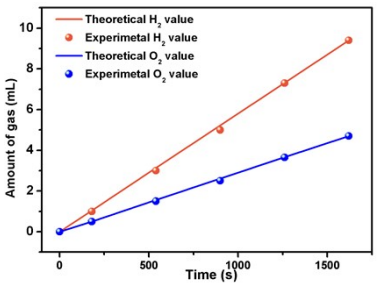

Figure S13. The volume of the gas changes with time.

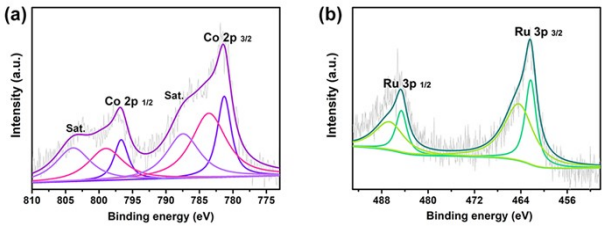

Figure S14. Co 2p and Ru 3p XPS spectras for m-CoRu@NC after HER cycles.

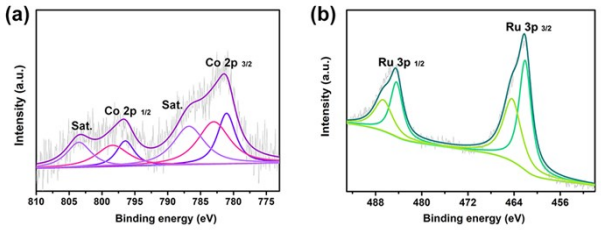

Figure S15. Co 2p and Ru 3p XPS spectras for m-CoRu@NC after OER cycles.

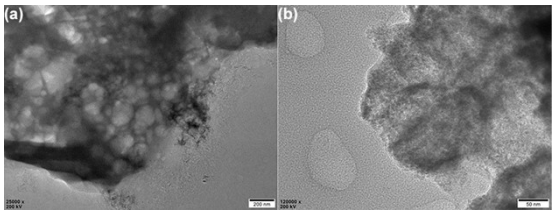

Figure S16. TEM images of m-CoRu@NC after HER cycles.

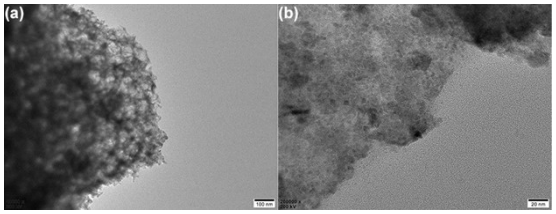

Figure S17. TEM images of m-CoRu@NC after OER cycles.

Table S1. Comparison of reported HER activities for various Ru-based electrocatalysts.

Catalyst	$\eta_{j=10\ mAcm^{-2}}$ (mV)	Tafel slope (mV dec^{-1})	C_{dl} (mF cm^{-2})	Ru (wt%)	Reference
m-CoRu@NC	9	47	31	0.85	This work
Ru@MWCNT	17	27	_	11.6	*Nat. Commun*. **2020**, *11*, 1278.
RuCoP	23	37	_	17.7	*Energy Environ. Sci*. **2018**, *11*, 1819-1827.
Ru@Ni-MOF	22	40	8.61	2.3	*Angew. Chem. Int. Ed*. **2021**, *60*, 22276-22282.
Ru/Co@OG	13	22.8	_	6.9	*Angew. Chem. Int. Ed*. **2021**, *60*, 16044-16050.
$CoRu_{0.5}$/CQDs	18	38.5	112.4	1.33	*Angew. Chem. Int. Ed*. **2021**, *60*, 3290-3298.
$Co_{0.87}Ru_{0.13}$/GC	14	71.7	41.35	0.93	*Chem. Eng. J*. **2021**, *417*, 128047.
$CoRu_{0.25}$@N-C	27	73	54.8	5.1	*ACS Sustainable Chem. Eng*. **2019**, *7*, 7014-7023.
RuCo@HCSs	21	32	53	1.8	*ACS sustainable Chem. Eng*. **2019**, *7*, 18744-18752.
Ru@Co/N-CNTs-2	48	33	4.0	0.71	*ACS Sustainable Chem. Eng*. **2020**, *8*, 9136-9144.
Ru-CoMo/CFP	44	37	165	0.53	*Appl. Surf. Sci*. **2021**, *541*, 148518
RuCo@CDs	11	47.8	170.15	7.82	*J. Mater. Chem. A* **2020**, *8*, 9638-9645.

Table S2. Comparison of overall water-splitting activities for various Ru-based electrocatalysts.

Catalyst	Cell Voltage (j_{10} V^{-1})	Reference
m-CoRu@NC	1.47	This work
Ru/c-$Ti_3C_2T_x$/NF	1.53	*Chem. Eng. J*. **2021**, *426*, 131234.
Ru-HPC	1.53	*Nano Energy* **2019**, *58*, 1-10.
Ru-$NiSe_2$/NF	1.537	*Small* **2022**, *18*, 2105305.
RuFe@NF	1.54	*J. Mater. Chem. A* **2022**, *10*, 4817-4824.
Ru-CoMo/CFP	1.54	*Appl. Surf. Sci*. **2021**, *541*, 148518.
Ru/RuO_2-MoO_2	1.54	*J. Colloid Interface Sci*. **2021**, *604*, 508-516.
RuCo@NC-750	1.54	*Electrochim. Acta* **2019**, *327*, 134958.
CoRu-O/A@HNC-2	1.558	*ACS Appl. Mater. Interfaces* **2020**, *12*, 51437-51447.
Ru/NF-2	1.56	*ACS Appl. Mater. Interfaces* **2020**, *12*, 36177-36185.
RuNi-NCNFs	1.564	*Adv. Sci*. **2020**, *7*, 1901833.
Ru_2Ni_2SNs/C	1.58	*Nano Energy*, **2018**, *47*, 1-7.
CoNG/Ru	1.58	*ACS Appl. Mater. Interfaces* **2019**, *11*, 46912-46919.
RuNi1Co1@CMT	1.58	*J. Colloid Interface Sci.* **2022**, *612*, 710-721.
Ru-doped CuO/MoS_2	1.68	*ACS Appl. Nano Mater.* **2021**, *4*, 7675-7685.

5. Theoretical calculation

The density functional theory (DFT) calculations were performed in the generalized gradient approximation (GGA) using the Perdew Burke ernzerhof (PBE) formula.[3-5] Projection enhanced wave (PAW) potential was used to describe the ion nucleus,[6,7] and 400 eV kinetic energy cutoff was employed for the plane wave basis set to consider the valence electrons. Using the Gaussian tailing method and a width of 0.05 eV, partial occupation of the Kohn sham orbit is allowed. When the energy change is less than 10^{-5} eV, the electron energy is considered to be self-consistent. The geometric optimization was considered to be convergent until the maximal residual force tolerance was less than 0.01 eV $Å^{-1}$.

The adsorption energies (E_{ads}) are calculated as $E_{ads} = E_{ad/sub} - E_{ad} - E_{sub}$, where $E_{ad/sub}$, E_{ad} and E_{sub} represent the optimized adsorbate/substrate system, the adsorbate in the structure and the clean substrate respectively.

The Gibbs free energy of hydrogen adsorption was calculated using the following equation, $\Delta G_{H^*} = \Delta E_{total} + \Delta E_{ZPE} - T\Delta S$, where E_{total}, E_{ZPE}, and S are the ground-state energy, zero-point energies and entropy respectively.

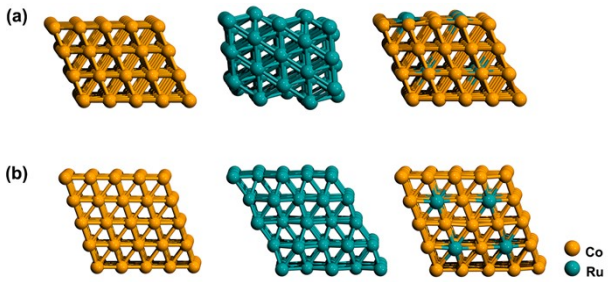

Figure S18. The side view (a) and top view (b) of DFT models for Co NP, Ru NP and CoRu nanoalloy.

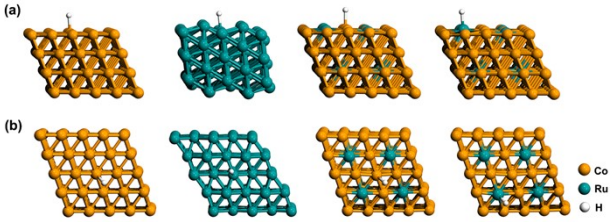

Figure S19. The side view (a) and top view (b) of chemisorption models of H on Co NP, Ru NP, Co@CoRu nanoalloy and Ru@CoRu nanoalloy.

	Co NP	**Ru NP**	**Co@CoRu nanoalloy**	**Ru@CoRu nanoalloy**
ΔG_{H^*} (eV)	-0.537	-0.401	-0.352	-0.217

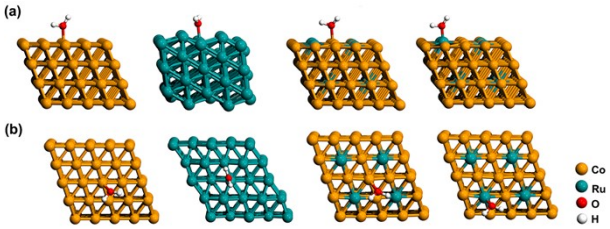

Figure S20. The side view (a) and top view (b) of chemisorption models of H_2O on Co NP, Ru NP, Co@CoRu nanoalloy and Ru@CoRu nanoalloy.

	Co NP	**Ru NP**	**Co@CoRu nanoalloy**	**Ru@CoRu nanoalloy**
E_{ads} **(eV)**	-0.61858	-0.91168	-1.53478	-2.01768

The typical Volmer-Heyrovsky process of HER in alkaline condition:

(1) $H_2O + M + e^- = M\text{-}H^* + OH^-$

(2) $H_2O + M\text{-}H^* + e^- = M + OH^- + H_2$

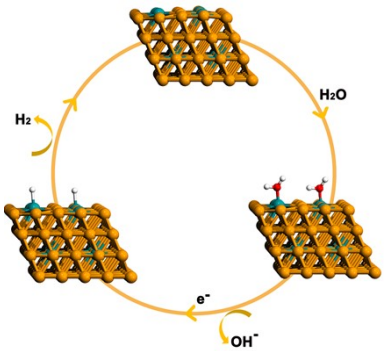

Figure S21. The proposed reaction mechanism for HER.

The typical process of OER in alkaline condition:

(1) $OH^- + M = M\text{-}OH^* + e^-$

(2) $M\text{-}OH^* + OH^- = H_2O + M\text{-}O^* + e^-$

(3) $OH^- + M\text{-}O^* = M\text{-}OOH^* + e^-$

(4) $OH^- + M\text{-}OOH^* = M + H_2O + O_2 + e^-$

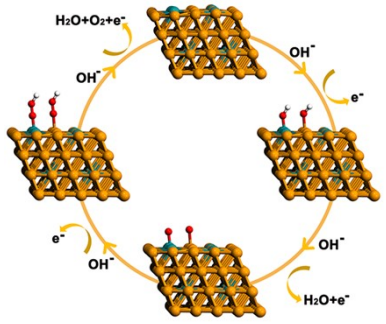

Figure S22. The proposed reaction mechanism for OER.

References

[1] H.-S. Yu, X.-J. Wei, J. Li, S.-Q. Gu, S. Zhang, L.-H. Wang, J.-Y. Ma, L.-N. Li, Q. GAO, R. Si, F.-F. Sun, Y. Wang, F. Song, H.-J. Xu, X.-H. Yu, Y. Zou, J.-Q. Wang, Z. Jiang, Y.-Y. Huang, *Nucl. Sci. Tech*. **2015**, *26*, 50102. The authors thank beamline BL14W1 (Shanghai Synchrotron Radiation Facility) for providing the beam time.

[2] K. Shen, L. Zhang, X. Chen, L. Liu, D. Zhang, Y. Han, J. Chen, J. Long, R. Luque, Y. Li, B. Chen, *Science* **2018**, *359*, 206-210.

[3] G. Kresse, J. Furthmüller, *Comput. Mater. Sci*. **1996**, *6*, 15-50.

[4] G. Kresse, J. Furthmüller, *Phys. Rev. B* **1996**, *54*, 11169-11186.

[5] J. P. Perdew, K. Burke, M. Ernzerhof, *Phys. Rev. Lett*. **1996**, *77*, 3865-3868.

[6] G. Kresse, D. Joubert, *Phys. Rev. B* **1999**, *59*, 1758-1775.

[7] P. E. Blöchl, *Phys. Rev. B* **1994**, *50*, 17953-17979.